ChemComm

COMMUNICATION

View Article Online
View Journal | View Issue

Cite this: *Chem. Commun.*, 2019, **55**, 13530

Received 24th September 2019,
Accepted 14th October 2019

DOI: 10.1039/c9cc07501a

rsc.li/chemcomm

Polymersomes with aggregation-induced emission based on amphiphilic block copolypeptoids†

Xinfeng Tao,[ab] Hui Chen,[b] Sylvain Trépout,[c] Jiayu Cen,[d] Jun Ling[d] and Min-Hui Li*[be]

Biocompatible polymersomes are prepared from amphiphilic block copolypeptoids with aggregation-induced emission, where the hydrophobic block P(TPE-NAG) is a tetraphenylethylene (TPE)-modified poly(*N*-allylglycine) and the hydrophilic block is polysarcosine. These nanoparticles are non-cytotoxic and show strong fluorescence emission in aqueous solution.

Nanoparticles composed of amphiphilic copolymers have attracted extensive attention in the past decades due to their ordered nanostructures with various morphologies, including spherical micelles, cylindrical micelles and vesicles, *etc.*, which can be potentially used in drug delivery and bioimaging systems.[1] Among them, polymer vesicles, also known as polymersomes, are cell-mimicking hollow spheres with a polymer bilayer membrane enclosing an aqueous volume in its interior. They are more stable and robust than lipid vesicles (liposomes) and have high encapsulation capacity for both hydrophilic and hydrophobic molecules.[2,3]

Polypeptoids are a class of poly(amino acid)s suitable for the preparation of polymersomes with the advantages of excellent biocompatibility, degradability, and low cytotoxicity.[4] Polypeptoids have a protein-mimicking structure with *N*-substituted glycine as repeating units but lack intramolecular and intermolecular hydrogen bonding along the amino acid backbone. Therefore, polypeptoids show better solubility, thermal processability, cell permeability and proteolytic stability compared to polypeptides.[4] Polypeptoids are usually synthesized by ring-opening polymerization (ROP) of *N*-substituted glycine *N*-carboxyanhydride (NNCA).[4] Recently, we developed an efficient alternative way to synthesize well-defined polypeptoids using a more stable monomer *N*-substituted glycine *N*-thiocarboxyanhydride (NNTA).[5]

Nanoparticles based on polypeptoids have been widely investigated.[6] Luxenhofer and co-workers prepared worm-like micelles and polymersomes by using amphiphilic block copolypeptoids containing a hydrophilic polysarcosine (PSar) block and a hydrophobic polypeptoid block with butyl, pentyl, benzyl or phenethyl side groups.[7] We reported previously that PSar-*block*-poly(ε-caprolactone)-*block*-PSar (PSar-*b*-PCL-*b*-PSar) formed unilamellar sheets, worm-like cylinders, and multilamellar polymersomes under different conditions.[8] Spherical micelles formed in water by poly(*N*-ethylglycine)-*block*-poly[(*N*-propargylglycine)-*r*-(*N*-decylglycine)] (PNEG-*b*-P(NPgG-*r*-NDG)) were studied by Zhang *et al.*[9] They used the hydrophobic core of micelles to encapsulate doxorubicin (DOX) for further applications of controlled release of DOX.[9] Sun *et al.* synthesized different PEG-*block*-polypeptoids which self-assembled into two-dimensional nanosheets.[10,11]

All the above reported nanoparticles are based on polypeptoids with normal aliphatic or aromatic side chains. Nevertheless, functional side chains are often required in various applications, for example, for the preparation of stimuli-responsive nanoparticles in controlled release or fluorescent nanoparticles in bioimaging. In a recent paper, we developed oxidation-responsive polymersomes based on copolypeptoids, poly(*N*-3-(methylthio)propyl glycine)-*block*-PSar (PMeSPG-*b*-PSar), containing thioether side-chains on PMeSPG.[12] However, this method has some limitations, *i.e.*, we need to develop a specific synthesis route for each functional monomer, which is tedious and time-consuming. In this study, we propose to use a functionalizable poly(*N*-allylglycine) (PNAG) as a hydrophobic block, which is an excellent platform for modification through a thiol–ene reaction to get functional polypeptoids.[13] PNAG-*b*-PSar was synthesized using benzylamine-initiated ROP of *N*-allylglycine NTA (NAG-NTA) and sarcosine NTA (Sar-NTA). To

[a] *Shanghai Key Laboratory of Advanced Polymeric Materials, School of Materials Science and Engineering, East China University of Science and Technology, Shanghai 200237, China*
[b] *Chimie ParisTech, PSL Université Paris, CNRS, Institut de Recherche de Chimie Paris, UMR8247, 11 rue Pierre et Marie Curie, 75005 Paris, France. E-mail: min-hui.li@chimieparistech.psl.eu*
[c] *Institut Curie, PSL Université Paris, INSERM U1196 and CNRS UMR9187, 91405 Orsay Cedex, France*
[d] *MOE Key Laboratory of Macromolecular Synthesis and Functionalization, Department of Polymer Science and Engineering, Zhejiang University, Hangzhou 310027, China*
[e] *Beijing Advanced Innovation Center for Soft Matter Science and Engineering, Beijing University of Chemical Technology, 15 North Third Ring Road, Chaoyang District, 100029 Beijing, China*

† Electronic supplementary information (ESI) available. See DOI: 10.1039/c9cc07501a

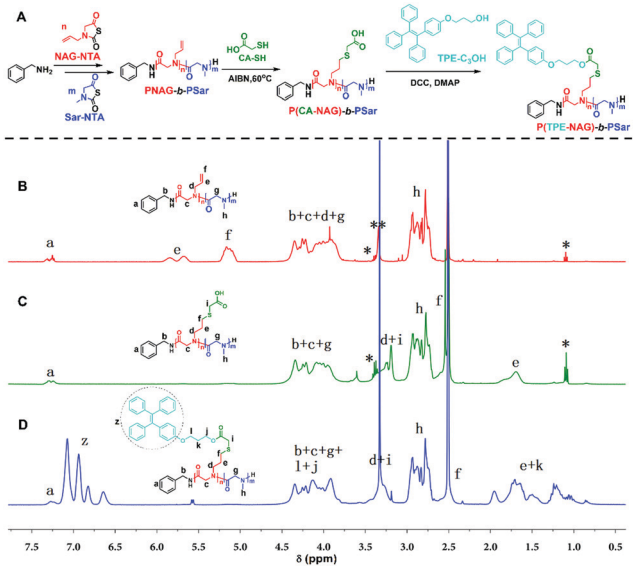

Fig. 1 (A) Synthesis of PNAG-*b*-PSar through block copolymerization of NAG-NTA and Sar-NTA and its postpolymerization modification by reaction with mercaptoacetic acid and TPE-C_3OH successively to produce P(TPE-NAG)-*b*-PSar. ^{1}H NMR spectra of $PNAG_{15}$-*b*-$PSar_{54}$ (B), $P(CA\text{-}NAG)_{15}$-*b*-$PSar_{54}$ (C) and $P(TPE\text{-}NAG)_{15}$-*b*-$PSar_{54}$ (D) in DMSO-d_6 (*: diethyl ether; **: water).

highlight their ability to be functionalized at their side-chains and to self-assemble into functional polymersomes, we attached tetraphenylethylene (TPE),[14–18] the emblematic luminogen with aggregation-induced emission (AIE), to PNAG side chains through postpolymerization modification (Fig. 1A). Polymersomes and micelles with AIE properties were obtained by using a nanoprecipitation method. Cytotoxicity tests showed good biocompatibility of these nanoparticles. We believe that these AIE polymersomes based on polypeptoids will have potential application in bio-imaging and drug delivery.

We first synthesized Sar-NTA and the novel monomer NAG-NTA through a phosgene-free method (Fig. S1–S6, ESI†).[5] Homopolymerization of NAG-NTA initiated by benzylamine in acetonitrile at 60 °C was then studied (Table S1, ESI†). The well-controlled characteristics of NAG-NTA polymerization based on single-site initiation by benzylamine were supported by MALDI-ToF mass spectra, ^{1}H NMR spectra and SEC traces (see ESI† and Fig. S8–S10 for details). PNAG can be modified easily through a thiol–ene radical addition reaction with mercaptan, *e.g.* mercaptoacetic acid, mercaptoethanol, and benzyl mercaptan (Scheme S5, ESI†). The ^{1}H NMR spectra (Fig. S9, ESI†) indicated the quantitative transformation of allyl groups to the selected functional groups.

PNAG-*b*-PSar with three different molecular weights were then synthesized by sequential feeding of different amounts of NAG-NTA and Sar-NTA (Fig. 1A). The successful synthesis of PNAG-*b*-PSar was proved by ^{1}H NMR spectra and SEC traces (see Fig. 1B and Fig. S11 and discussion in the ESI†). The compositions of the three block copolymers were $PNAG_{10}$-*b*-$PSar_{53}$, $PNAG_{15}$-*b*-$PSar_{54}$ and $PNAG_{25}$-*b*-$PSar_{46}$ as calculated from NMR data.

AIE luminogens were attached to the block copolymers by two-step reactions (Fig. 1A). PNAG-*b*-PSar was first reacted with mercaptoacetic acid (CA-SH) to get carboxylic acid-functionalized P(CA-NAG)-*b*-PSar (Fig. 1C), which was then reacted with 3-(4-(1,2,2-triphenylvinyl)phenoxy)propan-1-ol (TPE-C_3OH) (Scheme S4 and Fig. S7, ESI†) to get the AIE block copolymers P(TPE-NAG)-*b*-PSar. The final structures of P(TPE-NAG)-*b*-PSar were confirmed by ^{1}H NMR spectra (Fig. 1D and Fig. S12, ESI†) and SEC traces (Fig. S13, ESI†). Their molecular weights (MW) and distributions (*Đ*) are summarized in Table S2 (ESI†). The hydrophilic weight ratios (f_{PSar}) of P(TPE-NAG)-*b*-PSar are 18%, 30% and 38%, respectively.

$P(TPE\text{-}NAG)_{25}$-*b*-$PSar_{46}$ was chosen as an example to study the AIE properties of copolypeptoids. We found that it exhibited obvious AIE fluorescence when dispersed in water owing to the restriction of intramolecular rotation (RIM) of TPE moieties in the aggregated state (Fig. 2A and discussion in the ESI†).[18] Moreover, we were also interested in the morphology of aggregates formed in this experiment. The dispersion in a DMF/H_2O mixture with f_w = 99% was selected for DLS and cryo-EM analysis. Fig. 2B shows the size distribution of aggregates weighed by scattering intensity and by number. There are two populations of nanoparticles, where smaller ones with an average hydrodynamic diameter of about 56 nm is predominant and a few big particles with diameters >1000 nm co-exist. Fig. 2C and D show the nanostructures observed by cryo-EM, which confirm the results of DLS. Many nanoparticles with diameters <50 nm were observed. Note that hydrophilic chains located on the membrane coronas (exterior and interior sides) of the polymersomes are flexible and swollen in water, which do not constitute enough density contrast, relative to vitreous ice at the sample grid, to be visible in cryo-EM.[19] Therefore, it is

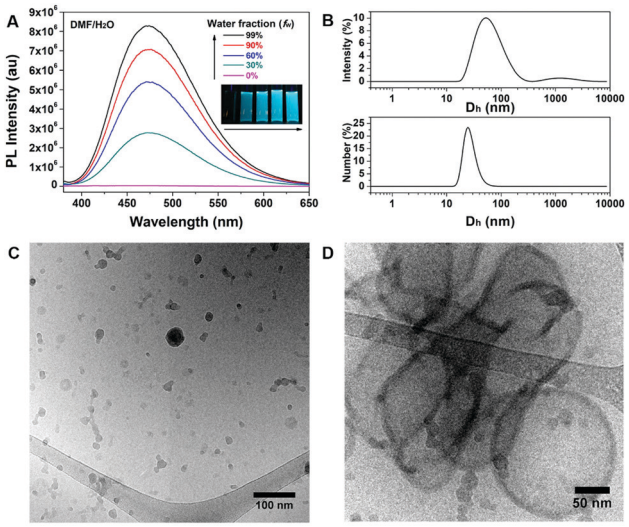

Fig. 2 (A) Photo-luminescence (PL) spectra of $P(TPE\text{-}NAG)_{25}$-*b*-$PSar_{46}$ in DMF/H_2O mixtures with different water fractions (concentration: 2.2 × 10^{-5} M, 0.4 mg mL^{-1}; excitation wavelength: 370 nm). The inserted photographs in (A) show samples with different water fractions under UV light at 365 nm. (B) DLS profiles (*Z*-average with intensity and number average) of aggregates of $P(TPE\text{-}NAG)_{25}$-*b*-$PSar_{46}$ in a DMF/H_2O mixture with a water fraction of 99%. (C and D) cryo-EM images of aggregates of $P(TPE\text{-}NAG)_{25}$-*b*-$PSar_{46}$ in a DMF/H_2O mixture with a water fraction of 99%.

normal that the sizes measured by cryo-EM are smaller than the hydrodynamic diameters. Meanwhile, a few vesicles (Fig. 2D and Fig. S15, ESI†) are also observed, and some of them have very big size, which corresponds effectively to the second population of particles in DLS curves. These observations showed that the copolypeptoid P(TPE-NAG)$_{25}$-*b*-PSar$_{46}$ had the tendency to form vesicular structures. However, well defined polymersomes were not obtained probably because of the quick addition of a large quantity of water.

Then, we used a nanoprecipitation method with DMF/water as the co-solvent and a slow water addition process to self-assemble P(TPE-NAG)-*b*-PSar in a more controlled way. Typically, P(TPE-NAG)-*b*-PSar was first dissolved in 1 mL DMF at a concentration of 2 mg mL^{-1}, and deionized water was then added very slowly (2.5 μL min^{-1}) with slight shaking. The slow rate of water addition could avoid the early freezing of the nanostructure and keep the self-assembly dynamic as long as possible. When the water content was increased to around 70% by volume, the dispersions were dialyzed against deionized water to remove DMF and get P(TPE-NAG)-*b*-PSar self-assemblies in pure water. Table S2 (ESI†) summarizes the hydrodynamic diameters of all nanoparticles and membrane thicknesses of the polymersomes. For P(TPE-NAG)$_{10}$-*b*-PSar$_{53}$ (f_{Psar} = 38%), micelles with a diameter of around 26 nm are mainly observed by cryo-EM (Fig. 3G and Fig. S16, ESI†) and TEM (Fig. S17, ESI†). The DLS intensity profile shows a bimodal distribution (Fig. 3A) with hydrodynamic diameters of 29 nm and 312 nm, respectively. When there are several populations of nanoparticles, it is difficult to quantify the statistics with only one kind of size profile in DLS because the intensity profile favours the big particles and the number profile favours the small particles. Therefore, both intensity-weighed and number-weighed DLS curves are given here (Fig. 3A and D). The smaller one corresponds to the micelles, while the larger one (very few in number as shown in the number profile of DLS) may be attributed to a few aggregates (clusters) of micelles (Fig. 3G and Fig. S16, ESI†). When the f_{Psar} decreases to 30% (P(TPE-NAG)$_{15}$-*b*-PSar$_{54}$), both micelles and polymersomes were observed by cryo-EM (Fig. 3H and Fig. S18, ESI†) and TEM (Fig. S19, ESI†), whose diameters are 26 nm and 357 nm, respectively. The DLS profiles of P(TPE-NAG)$_{15}$-*b*-PSar$_{54}$ nanoparticles show double peaks with hydrodynamic diameters of 38 nm and 203 nm (Fig. 3B), which is consistent with the TEM results. Note that the polymersomes were a minor population as shown in the DLS number profile and connected or fused polymersomes were observed in some cases (Fig. S18, ESI†). In the case of PNAG$_{25}$-*b*-PSar$_{46}$ (f_{Psar} = 18%), only polymersomes are formed according to cryo-EM images (Fig. 3I and Fig. S20, ESI†), with two distributions of sizes: one around a *Z*-average diameter of 804 nm, and another around a *Z*-average diameter of 136 nm as measured by DLS (Fig. 3C and F). As for the sizes and size distributions, the results obtained from cryo-EM and DLS (Table S2, ESI†) are coherent to some extent.

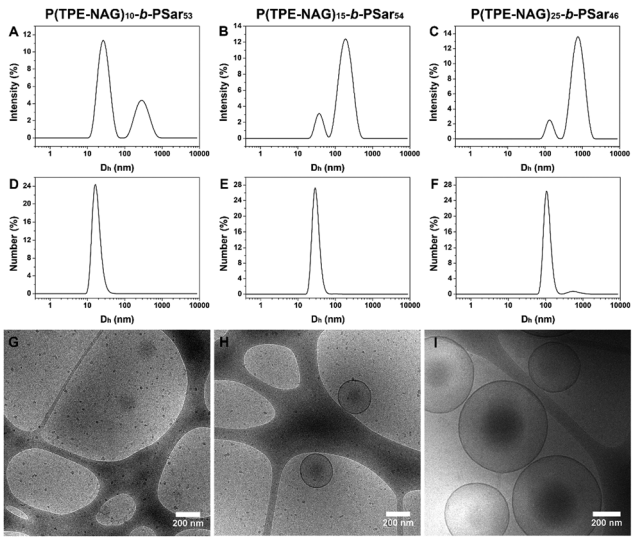

Fig. 3 DLS profiles (*Z*-average with intensity (A–C) and number average (D–F)) and cryo-EM images of nanoparticles in water formed by P(TPE-NAG)$_{10}$-*b*-PSar$_{53}$ (f_{Psar} = 38%) (A, D and G), P(TPE-NAG)$_{15}$-*b*-PSar$_{54}$ (f_{Psar} = 30%) (B, E and H) and P(TPE-NAG)$_{25}$-*b*-PSar$_{46}$ (f_{Psar} = 18%) (C, F and I). The dark densities present at the center of the polymersomes are caused by the scattering of electrons due to the inherent thickness of the polymersome spheres.

With the increase of the hydrophobic P(TPE-NAG) chain length and the decrease of the hydrophilic ratio f_{Psar} (here the length of the hydrophilic part PSar is similar for three copolypeptoids), the nanostructures transform from micelles to vesicles and their average sizes become larger. These tendencies can be empirically explained by the increase of the packing parameter $p = v/al$ (v is the hydrophobic volume, a is the optimal interfacial area and l is the length of the hydrophobic block normal to the interface) when increasing the hydrophobic block MW, as already reported previously.[15,20,21]

According to the cryo-EM images, the thickness of the hydrophobic part of the membrane is measured to be 8 ± 1 nm and 10 ± 1 nm for P(TPE-NAG)$_{15}$-*b*-PSar$_{54}$ and P(TPE-NAG)$_{25}$-*b*-PSar$_{46}$ polymersomes, respectively. By using the MM2 energy minimization with the Chem3D software, the contour lengths of the hydrophobic part P(TPE-NAG)$_{15}$ and P(TPE-NAG)$_{25}$ are about 4.4 nm and 7.3 nm, respectively. Consequently, a perfectly-ordered tail-to-tail bilayer should have a membrane thickness of 8.8 nm and 14.6 nm, respectively. The membrane thickness measured by cryo-EM is lower than the double lengths of two extended P(TPE-NAG) chains. Therefore, the obtained polymersomes should be unilamellar vesicles, in which the P(TPE-NAG) chains might not be totally extended or might be interdigitated between the two leaflets.

Then, we investigated the fluorescence of these well-defined nanostructures formed by P(TPE-NAG)-*b*-PSar. The DMF solution of P(TPE-NAG)-*b*-PSar is non-emissive while the aqueous solution of P(TPE-NAG)-*b*-PSar micelles and vesicles shows strong emission under a 365 nm UV lamp (Fig. 4A) due to the RIM of TPE moieties in the core of polymer micelles and the polymersome membrane as expected. The emission spectra of the P(TPE-NAG)$_{10}$-*b*-PSar$_{53}$, P(TPE-NAG)$_{15}$-*b*-PSar$_{54}$ and P(TPE-NAG)$_{25}$-*b*-PSar$_{46}$ nanoparticles are shown in Fig. 4B with maximal emission wavelengths of 478 nm, 474 nm and 471 nm, respectively, the excitation wavelength being set as 370 nm which corresponded to the maximal wavelength in the excitation spectrum (Fig. S21, ESI†). Rather high

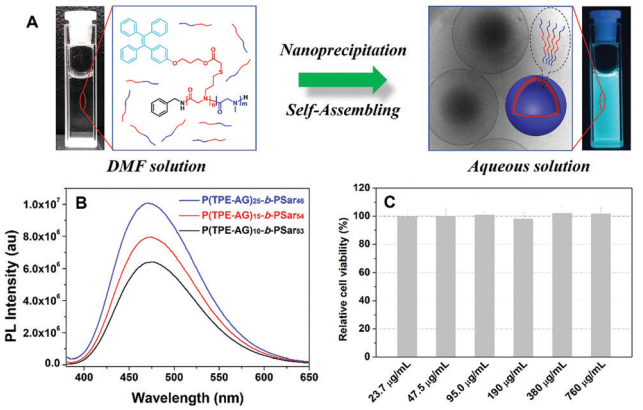

Fig. 4 (A) Schematic diagram of the self-assembly of P(TPE-NAG)-*b*-PSar in aqueous solution and the AIE phenomenon of the polymersome dispersion. (B) PL spectra of different nanoparticles (concentration: 0.4 mg mL^{-1}; excitation wavelength: 370 nm). (C) Relative cell viability of P(TPE-NAG)$_{25}$-*b*-PSar$_{46}$ polymersomes for human vein endothelial cells after 24 h incubation at a concentration of 23.7 μg mL^{-1}, 47.5 μg mL^{-1}, 95.0 μg mL^{-1}, 190 μg mL^{-1}, 380 μg mL^{-1} and 760 μg mL^{-1}, respectively.

quantum yields of 26%, 29% and 34% were measured for P(TPE-NAG)$_{10}$-*b*-PSar$_{53}$, P(TPE-NAG)$_{15}$-*b*-PSar$_{54}$ and P(TPE-NAG)$_{25}$-*b*-PSar$_{46}$ nanoparticles, respectively, using the integrating sphere method. The fluorescence intensity and quantum yield increase following the morphology evolution from micelles, micelles/polymersomes to polymersomes, which is attributed to the increasing packing density of the polymer blocks within the nanoparticles and the increasing confinement of the AIEgens.[14]

Finally, the biocompatibility of the nanoparticles was assessed by using the MTT cell viability assay.[22] Human vein endothelial cells were incubated for 24 h with P(TPE-NAG)-*b*-PSar nanoparticles at different concentrations. All P(TPE-NAG)-*b*-PSar micelles and polymersomes studied are non-cytotoxic (Fig. 4C and Fig. S22, S23, ESI†), indicating their excellent biocompatibility. The negligible cytotoxicity of P(TPE-NAG)-*b*-PSar polymersomes enables their application in bio-related domains such as bio-imaging and drug delivery.

In summary, *N*-allylglycine NTA was synthesized for the first time, whose corresponding polymer PNAG is an excellent platform for post-modification to produce different functional polypeptoids. Well-controlled polymerization of NAG-NTA was achieved by using primary amine as the initiator, and PNAGs with narrow distributions were produced. A series of diblock copolypeptoids PNAG-*b*-PSar with different chain lengths were synthesized by sequential feeding of NAG-NTA and Sar-NTA. TPE-functionalized P(TPE-NAG)$_{10}$-*b*-PSar$_{53}$ (f_{Psar} = 38%), P(TPE-NAG)$_{15}$-*b*-PSar$_{54}$ (f_{Psar} = 30%) and P(TPE-NAG)$_{25}$-*b*-PSar$_{46}$ (f_{Psar} = 18%) were prepared by a post-polymerization reaction. Self-assembly was performed by a nanoprecipitation method using DMF/water as the co-solvent. Micelles, micelles/polymersomes and polymersomes were obtained for P(TPE-NAG)$_{10}$-*b*-PSar$_{53}$, P(TPE-NAG)$_{15}$-*b*-PSar$_{54}$ and P(TPE-NAG)$_{25}$-*b*-PSar$_{46}$, respectively. All the nanoparticles show strong AIE fluorescence in aqueous solution. These AIE polymer micelles and AIE polymersomes made of block copolypeptoids are non-cytotoxic, which guarantees their safety in potential applications in bio-related fields.

Financial support from French National Research Agency (ANR-16-CE29-0028) and the National Natural Science Foundation of China (21674091) is acknowledged. We thank Prof. Ben Zhong Tang (Hong Kong University of Science and Technology) for fruitful discussions. We thank Prof. Zhengwei Mao (Zhejiang University) for cytotoxicity analysis, and Dr Chao Deng (Zhejiang University) for quantum yield measurement. The authors thank the PICT-Ibisa for providing access to the cryo-EM facility at Institut Curie in Orsay.

Conflicts of interest

There are no conflicts to declare.

Notes and references

1 Y. Mai and A. Eisenberg, *Chem. Soc. Rev.*, 2012, **41**, 5969–5985.
2 Y. Deng, J. Ling and M.-H. Li, *Nanoscale*, 2018, **10**, 6781–6800.
3 E. Rideau, R. Dimova, P. Schwille, F. R. Wurm and K. Landfester, *Chem. Soc. Rev.*, 2018, **47**, 8572–8610.
4 N. Gangloff, J. Ulbricht, T. Lorson, H. Schlaad and R. Luxenhofer, *Chem. Rev.*, 2016, **116**, 1753–1802.
5 X. F. Tao, M.-H. Li and J. Ling, *Eur. Polym. J.*, 2018, **109**, 26–42.
6 A. Birke, J. Ling and M. Barz, *Prog. Polym. Sci.*, 2018, **81**, 163–208.
7 C. Fetsch, J. Gaitzsch, L. Messager, G. Battaglia and R. Luxenhofer, *Sci. Rep.*, 2016, **6**, 33491.
8 Y. W. Deng, T. Zou, X. F. Tao, V. Semetey, S. Trepout, S. Marco, J. Ling and M. H. Li, *Biomacromolecules*, 2015, **16**, 3265–3274.
9 A. Li and D. H. Zhang, *Biomacromolecules*, 2016, **17**, 852–861.
10 Z. Shi, Y. Wei, C. Zhu, J. Sun and Z. Li, *Macromolecules*, 2018, **51**, 6344–6351.
11 Y. Wei, J. Tian, Z. Zhang, C. Zhu, J. Sun and Z. Li, *Macromolecules*, 2019, **52**, 1546–1556.
12 Y. W. Deng, H. Chen, X. F. Tao, F. Y. Cao, S. Trépout, J. Ling and M.-H. Li, *Biomacromolecules*, 2019, **20**, 3435–3444.
13 J. W. Robinson and H. Schlaad, *Chem. Commun.*, 2012, **48**, 7835–7837.
14 M. Huo, Q. Q. Ye, H. L. Che, X. S. Wang, Y. Wei and J. Y. Yuan, *Macromolecules*, 2017, **50**, 1126–1133.
15 N. Zhang, H. Chen, Y. Fan, L. Zhou, S. Trepout, J. Guo and M.-H. Li, *ACS Nano*, 2018, **12**, 4025–4035.
16 D. Zhang, Y. Fan, H. Chen, S. Trépout and M.-H. Li, *Angew. Chem., Int. Ed.*, 2019, **58**, 10260–10265.
17 Q. Liu, Q. Xia, S. Wang, B. S. Li and B. Z. Tang, *J. Mater. Chem. C*, 2018, **6**, 4807–4816.
18 S. Liu, Y. Cheng, H. Zhang, Z. Qiu, R. T. K. Kwok, J. W. Y. Lam and B. Z. Tang, *Angew. Chem., Int. Ed.*, 2018, **57**, 6274–6278.
19 G. H. Michler, *Electron Microscopy of Polymers*, Springer, Berlin, 2008.
20 A. Blanazs, S. P. Armes and A. J. Ryan, *Macromol. Rapid Commun.*, 2009, **30**, 267–277.
21 L. Jia, P.-A. Albouy, A. Di Cicco, A. Cao and M.-H. Li, *Polymer*, 2011, **52**, 2565–2575.
22 G. Yu, S. Yu, M. L. Saha, J. Zhou, T. R. Cook, B. C. Yung, J. Chen, Z. Mao, F. Zhang, Z. Zhou, Y. Liu, L. Shao, S. Wang, C. Gao, F. Huang, P. J. Stang and X. Chen, *Nat. Commun.*, 2018, **9**, 4335.